

Stability and Vibration Analysis of Porous Axially Graded Pipe Conveying-Fluid Lying on Pasternak Foundation



Zahraa Qassim Jerad , Talib Ehraize Elaikh* , Ahmed Abdul-Hussein Ouda 

Department of Mechanical Engineering, College of Engineering, University of Thi-Qar, Thi-Qar 64001, Iraq

Corresponding Author Email: talib-h@utq.edu.iq

Copyright: ©2025 The authors. This article is published by IIETA and is licensed under the CC BY 4.0 license (<http://creativecommons.org/licenses/by/4.0/>).

<https://doi.org/10.18280/ijht.430137>

ABSTRACT

Received: 8 November 2024

Revised: 29 January 2025

Accepted: 14 February 2025

Available online: 28 February 2025

Keywords:

axially functionally graded (AFG), Pasternak foundation, pipe conveys fluid, porosity, Galerkin method (GM)

This paper investigates the stability of an axially functionally graded (AFG) pipe carrying fluid flow supported by two elastic foundations and constrained by double-clamped end conditions. Hamilton's principle provides the vibration equations, while the Galerkin procedure discretizes the system equation to facilitate analysis of the dynamic behaviour. The pipe's mechanical properties vary along the axial direction according to a power-law distribution. The model incorporates the effects of different porosity, axial grading, fluid velocity, and foundation stiffness on the system's dynamic behaviour. Numerical results show that an increase in fluid velocity by 20% results in a 30% reduction in the first frequency, indicating enhanced system instability. Additionally, modules of elasticity ratio significantly influence the natural frequencies, with variations in gradient index leading to a 19% increase in the system's fundamental frequency. The Pasternak foundation provided a stabilizing effect, with a 20% increase in foundation stiffness, improving the stability margin by 25%. These findings show that porosity, axial grading, and foundation parameters play important roles in determining fluid-conveying pipes' vibration characteristics and stability.

1. INTRODUCTION

The vibration behaviour of fluid-conveying pipes exemplifies fluid-solid coupling phenomena. These slender structures find extensive application in various engineering sectors, such as marine engineering, nuclear power, aerospace, and petrochemical industries. As a result, studying the dynamics of these systems holds substantial engineering and academic significance, making them a topic of considerable interest to researchers [1]. Giacobbi et al. [2] employed the finite element method to inspect the impact of longitudinally varying density on the dynamics behaviour of pipes flowing fluid with clamped and cantilevered boundary conditions. The dynamic analysis of Rayleigh pipes with flowing fluid and non-classical boundary conditions was carried out by Dagli and Ergut [3]. Xu et al. [4] computed the complex vibration of a viscoelastic fluid-conveying clamped pipe using the differential quadrature (DQ) method. Zhao et al. [5] employed DTM and Galerkin discretization to conduct the dynamics of the pipe-carrying fluid.

In petroleum engineering, pipelines frequently traverse challenging terrains, including sand, gravel, soil, and mixed environments, during the conveyance of oil and gas. As a result, the flow of oil or gas through these pipes in challenging environments makes them susceptible to unstable vibrations. This has sparked significant interest in studying the stability of pipes conveying fluid supported by elastic foundations under various boundary conditions. Ma et al. [6] investigated the vibration stability of a pipe-carrying fluid supported by a two-

parameter foundation using the HDQ method. Li et al. [7] utilized Green's function to obtain an explicit solution for the vibrations of oil-conveying pipes supported by Pasternak foundations. Askarian et al. [8] examined the stability of pipes translating fluid lying on a viscoelastic foundation. Hamilton's fundament was employed to acquire the pipe motion equation and solve it through the Galerkin method (GM). A fluid-conveying pipe lying on the Winkler-Pasternak foundation was studied [9]. Using the semi-analytic solution, they determined the system's critical velocities and complex frequencies. Wu et al. [10] proposed the dynamic stiffness (DS) method for examining the impact of Pasternak foundation parameters on the stability of pipes that convey fluid across multiple spans.

Additionally, functionally graded materials (FGMs) are innovative composite materials with properties that gradually change across spatial positions, enabling the customization of material characteristics by controlling the distribution of volume fractions. These materials exhibit significantly enhanced performance over conventional materials, particularly in fracture toughness and wear resistance [11]. Axial FGMs have properties that change along their length, enabling them to be tailored for specific performance under dynamic and thermal loads, such as those encountered in fluid-conveying pipes. Different preparation techniques, such as powder metallurgy, laser melting deposition (LMD), slip casting, and electrochemical deposition, were used to fabricate axial FGM pipes. However, most research on FGMs has been concentrated on beams, plates, and shells [12-14], with

comparatively limited studies addressing the dynamic behaviour of FGM pipelines used for fluid transport. Cao [15] conducted the impact of random foundations on the critical velocity of FGM pipes under thermal stress using (FEM). Ma and Mu [16] determined the influence of multiple physical fields on the stability of FGM simply supported microtubes. The governing equation for these microtubes was obtained using Hamilton's principle with the conjugate of strain gradient theory. Guo et al. [17] proposed an effective statistical method for flow pipeline systems constructed with random axial functional gradient materials. Ihmood and Al-Umar [18] studied the stability of fluid-flow pipes made of new inhomogeneous materials. El and Ihmood [19] established a linear vibration model of FGM flow pipes on visco-elastic foundations. The linear frequency and stability were determined using DQM. Selmi and Hassis [20] analyzed the vibration of the fluid-conveying pipeline made of functional gradient materials and obtained the exact solution under different boundary conditions. Deng et al. [21] studied the stability of viscoelastic functional gradient material pipelines. They explored the influence of volume fraction index, fluid velocity, and internal damping on the dynamic of the pipeline system. Wang and Liu [22] studied the impact of gradient material on wall thickness for lateral vibration problems of pipeline conveying fluid. An and Su [23] used the generalized integral (GI) transform technique to numerically study the dynamic behaviour of the axial functional gradient pipeline conveying fluid. Zhao et al. [24] investigated the vibration characteristic of functionally graded conical fluid-conveying pipes utilizing DQM. Elaikh et al. [25] addressed the natural frequency of FGM double micro-pipelines using the GM.

Furthermore, pores and micropores can form in FGMs during the manufacturing process, which may negatively affect the mechanical characteristics of the structures. However, when the porosity distribution is optimized, it can enhance mechanical and structural properties such as energy dissipation, strength, and stiffness [26]. As a result, porous functionally graded material pipelines for fluid transport have been extensively utilized in engineering applications like nuclear reactors and aerospace. However, little research has been done to explore how these pores impact linear or nonlinear responses of fluid-conveying FGM pipelines. Li et al. [27] employed the multiple-scale method to examine the nonlinear resonance of porous FGM pipes translating fluid. Zhou et al. [28] studied the influence of porosities on the dynamic response of fluid-conveying porous pipes made of radially graded materials. Khodabakhsh et al. [29] calculated the nonlinear stability of FGM Timoshenko model pipelines with uniform porosity and variable end conditions using an exact closed-form solution.

Previous reviews have revealed that most researchers have focused on the vibration analysis of composite pipes with transverse or axial gradients. However, the dynamic behaviour of porous functionally graded (FG) pipes with longitudinal gradients resting on an elastic foundation remains unexplored. This paper addresses this gap by investigating the dynamic characteristics of fluid-conveying FG pipes graded in the axial direction. Using Hamilton's principle, the governing equations for functionally graded material (FGM) double-clamped pipes are formulated and solved using the Galerkin technique. The study examines the effects of foundation parameters, gradient index, flow velocity, and modulus ratio on the vibration frequencies and stability of the system.

2. MATHEMATICAL FORMULATION

In Figure 1, the model of the AFG pipe carrying the fluid flow is shown. The length, inner radius, and outer radius of the Pipe are denoted by L , r_i and r_o , respectively, while U represents the velocity of fluid flow.

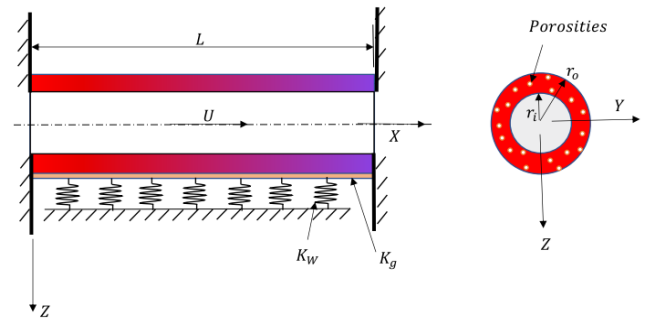


Figure 1. Scheme diagram of clamped AFG porosity pipe

2.1 Axially graded pipe properties

FGM pipes with uniform porosity are assumed to have linear properties longitudinally. This variation is governed by a power law function, where the properties change progressively from one material at one end of the pipe to another at the opposite end, as described by the study [30]:

$$E(x) = E_L E_X \quad (1)$$

$$\rho(x) = \rho_L \rho_X \quad (2)$$

in which,

$$E_X = 1 + (\bar{\alpha}_E - 1) \left(\frac{x}{L}\right)^k - \frac{\lambda}{2} (\bar{\alpha}_E + 1), \quad (3)$$

$$\rho_X = 1 + (\bar{\alpha}_\rho - 1) \left(\frac{x}{L}\right)^k - \frac{\lambda}{2} (\bar{\alpha}_\rho + 1), \quad (4)$$

In this context, ($\bar{\alpha}_E = E_R/E_L$ and $\bar{\alpha}_\rho = \rho_R/\rho_L$) represent the modulus and density ratios of the pipe's material properties. k is a positive value that describes the variation in material along the Pipe's length.

Figure 2 depicts the variation of the effective modulus ratio ($\frac{E(x)}{E_L}$) in the length direction for the FG pipe with $E_R = 3 E_L$.

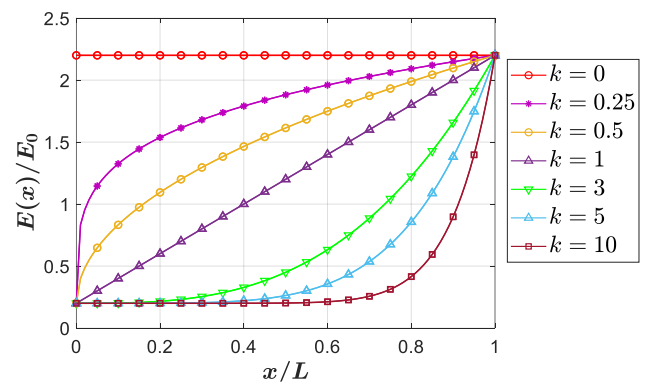


Figure 2. Variation of effective property $E(x)/E_L$ versus pipe length for AFGM pipe with various power index k values

2.2 Governing equations

The displacements (u_x , u_y and u_z) along directions of X, Y, and Z for any pipe point are determined as outlined [28].

$$\left. \begin{aligned} u_x(x, z, t) &= u(x, t) - z \frac{\partial w(x, t)}{\partial x} \\ u_y(x, z, t) &= 0 \\ u_z(x, z, t) &= w(x, t) \end{aligned} \right\} \quad (5)$$

In relation (5), w and z are the displacement of the pipe's middle and neutral plane coordinates, respectively, while t stands for the time.

Accordingly, the longitudinal strain resulting from pipe displacement can be expressed as:

$$\varepsilon_{xx} = \frac{\partial u}{\partial x} + \frac{1}{2} \left(\frac{\partial w}{\partial x} \right)^2 - z \frac{\partial^2 w}{\partial x^2} \quad (6)$$

The stress-strain relation for a pipeline with elastic properties is as follows:

$$\sigma_{xx} = E(x) \varepsilon_{xx} \quad (7)$$

An expression for the strain energy of FG pipelines is written as:

$$U_S = \int_V \sigma_{xx} \varepsilon_{xx} dV. \quad (8)$$

From inserting Eqs. (1), (6), and (7) in Eqs. (8) one can obtain the following:

$$U_S = \frac{1}{2} \int_0^L \left\{ E(x) A \left(\frac{\partial u}{\partial x} + \frac{1}{2} \left(\frac{\partial w}{\partial x} \right)^2 \right)^2 + E(x) I \left(\frac{\partial^2 w}{\partial x^2} \right)^2 \right\} dx \quad (9)$$

The system kinetic energy is calculated as:

$$T = \frac{1}{2} m_f \int_0^L \left[\left(U + \frac{\partial u}{\partial x} + U \frac{\partial u}{\partial x} \right)^2 + \left(\frac{\partial w}{\partial t} + U \frac{\partial w}{\partial t} \right)^2 \right] dx + \frac{1}{2} \int_0^L \rho(x) A \left[\left(\frac{\partial u}{\partial t} \right)^2 + \left(\frac{\partial w}{\partial t} \right)^2 \right] dx \quad (10)$$

Further, the reaction force of the Pasternak Foundation performs virtual work as follows:

$$\delta W = \int_0^L \left(-K_W w + K_G \frac{\partial^2 w}{\partial x^2} \right) \delta w dx \quad (11)$$

The dynamic control equations of the pipe can be obtained by enforcing Hamilton's generalized law:

$$\delta \int_{t_1}^{t_2} (T - U_S + W) dt = 0 \quad (12)$$

By replacing the kinetic energy, potential, and work of the external force in Eq. (12), the control equations will be obtained as follows:

$$\frac{\partial^2}{\partial x^2} \left[E(x) I \frac{\partial^2 w}{\partial x^2} \right] + (m_f + \rho(x) A) \frac{\partial^2 w}{\partial t^2} + 2m_f U \frac{\partial^2 w}{\partial x \partial t} + m_f U^2 \frac{\partial^2 w}{\partial x^2} + K_W w - K_G \frac{\partial^2 w}{\partial x^2} = 0 \quad (13)$$

The boundary condition equation for C-C is written as:

$$\left. \begin{aligned} w(0, t) &= \frac{\partial w(0, t)}{\partial x} = 0, & \text{at } x = 0 \\ w(L, t) &= \frac{\partial w(L, t)}{\partial x} = 0, & \text{at } x = L \end{aligned} \right\} \quad (14)$$

The following non-dimensional quantities are employed to simplify the subsequent control equation analysis.

$$\left. \begin{aligned} \xi &= \frac{x}{L}, \quad \eta = \frac{w}{L}, \quad k_w = \frac{K_W L^4}{E_L I}, \quad k_g = \frac{K_G L^2}{E_L I}, \\ \beta &= \frac{m_f}{m_f + \rho_L A}, \quad \tau = \sqrt{\frac{E_L I}{(m_f + \rho_L A) L^2}} t, \quad u = \sqrt{\frac{m_f}{E_L I}} U L \end{aligned} \right\} \quad (15)$$

By placing these parameters in Eq. (13), the dimensionless system's equations will be obtained:

$$\frac{\partial^2}{\partial \xi^2} (E_x \frac{\partial^2 \eta}{\partial \xi^2}) + (u^2 - k_g) \frac{\partial^2 \eta}{\partial \xi^2} + 2\sqrt{\beta} u \frac{\partial^2 \eta}{\partial \xi \partial \tau} + k_w \eta + (\beta + (1 - \beta) \rho_x) \frac{\partial^2 \eta}{\partial \tau^2} = 0 \quad (16)$$

The boundary conditions (Eq. (14)) are also written in a non-dimensional form as follows:

$$\left. \begin{aligned} \text{At } \xi = 0 &\rightarrow \eta(\xi) = 0, \quad \frac{\partial \eta(\xi)}{\partial \xi} = 0 \\ \text{At } \xi = 1 &\rightarrow \eta(\xi) = 0, \quad \frac{\partial \eta(\xi)}{\partial \xi} = 0 \end{aligned} \right\} \quad (17)$$

2.3 Methods of solution

In this study, the GM will be employed to find the vibration characteristics of the AFGM pipe. Through this method, the system equation (3-30) is transformed into an ordinary differential (OD) equation, and we can assume the displacement function ($\eta(\xi, \tau)$) of the FG pipe as [31, 32]:

$$\eta(\xi, \tau) = \sum_{j=1}^N \phi_j(\xi) q_j(\tau) \quad (18)$$

where, N is the mode number to be considered, $q_j(\tau)$ is the j th the time-dependent function, and $\phi_j(\xi)$ is the j th eigenfunction of the pipe. The mode shape standards for the SS boundary condition are provided as follows [33]:

$$\phi_j(\xi) = \cosh \lambda_j \xi - \cos \lambda_j \xi - \left(\frac{\cos \lambda_j - \cosh \lambda_j}{\sin \lambda_j - \sinh \lambda_j} \right) (\sinh \lambda_j \xi - \sin \lambda_j \xi) \quad (19)$$

Substituting Eq. (18) into Eq. (16) and multiplying the resulting expression by $\phi_k(\xi)$, and then integrating the obtained expression for x from zero to L , the system equation is obtained in general matrix form [34, 35]:

$$[M]_{N \times N} \ddot{q} + [C]_{N \times N} \dot{q} + [K]_{N \times N} q = 0 \quad (20)$$

in which,

$$\left. \begin{aligned} [M]_{jk} &= \int_0^1 (\beta + (1 - \beta) \rho_x) \phi_j(\xi) \phi_k(\xi) d\xi \\ [C]_{jk} &= 2\sqrt{\beta} u \int_0^1 \phi_j^{(1)}(\xi) \phi_k(\xi) d\xi \\ [K]_{jk} &= \int_0^1 E_x \phi_j^{(4)}(\xi) \phi_k(\xi) d\xi + \\ & 2 \int_0^1 E_x' \phi_j^{(3)}(\xi) \phi_k(\xi) d\xi + \\ & \int_0^1 E_x^{(2)} \phi_j^{(2)}(\xi) \phi_k(\xi) d\xi + (u^2 - \\ & K_g) \int_0^1 \phi_j^{(2)}(\xi) \phi_k(\xi) d\xi + K_w \int_0^1 \phi_j(\xi) \phi_k(\xi) d\xi \end{aligned} \right\} \quad (21)$$

Eq. (21) is transformed into a first-order state equation, facilitating the solution of all system modes using MATLAB software. The system's dynamic characteristics are evaluated through eigenvalue analysis. In this context, the eigenfrequency is expressed as a complex value: the real part represents the system's damping, while the imaginary part corresponds to its frequency.

3. RESULTS AND DISCUSSION

This section presents a comparative study to assess the proposed method's accuracy. It also further elucidates the impact of foundation parameters, density variations, and material gradations along the pipe length on the stability behaviour of the system boundaries.

In the analytical examples, the geometric parameters for the pipe are consistent with those specified in the study of Zhao et al. [24]: $d_o=80$ mm, $h=8$ mm, and $L=15$ m, the fluid density $\rho_f = 1000$ kg/m³. The fluid-conveying pipe material is composed of metal (**Ti-6Al-4V**) at the left side and ceramic (**SiC**) at the right side. Table 1 displays the properties of pipe materials.

Table 1. AFG pipe material properties [24]

Materials	E (GPa)	ρ (kg/m ³)	G (GPa)
SiC	440	3210	188
Ti-6Al-4V	115	4515	44.57

3.1 Validation of the model

The vibration of a homogeneous pipe on the Pasternak foundation was analyzed to validate the Galerkin solution presented in this paper. Two examples were considered for this validation. The governing equation for the pipe is as follows:

$$EI \frac{\partial^4 w}{\partial x^4} + (m_f + \rho A) \frac{\partial^2 w}{\partial t^2} + 2m_f u \frac{\partial^2 w}{\partial x \partial t} + m_f u^2 \frac{\partial^2 w}{\partial x^2} + k_w w - k_g \frac{\partial^2 w}{\partial x^2} = 0 \quad (22)$$

The first example considers a pipe carrying fluid without foundation experiencing transverse vibrations, is considered. The results for the first three vibrational modes are compared with the semi-analytical solution DQM [9], as shown in Figure 3. In the second example, the complex eigenvalues of the first three modes of the homogeneous pipe on an elastic foundation are compared with the DTM solution presented [36], as illustrated in Figure 4. The findings of this study align well with those reported in the previously mentioned literature.

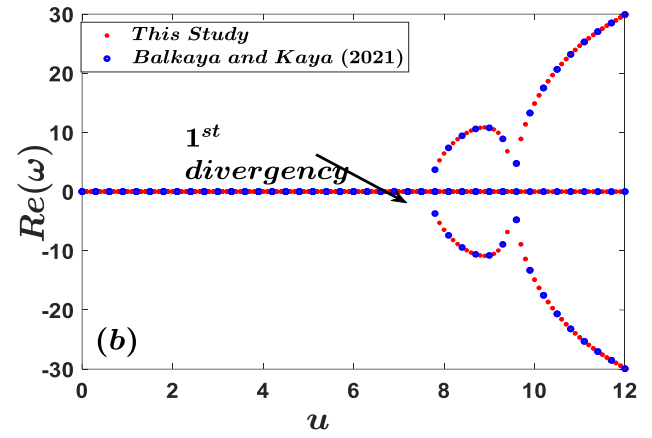


Figure 3. The first three modes of dimensionless frequency versus fluid velocity (u) of pipe conveying fluid

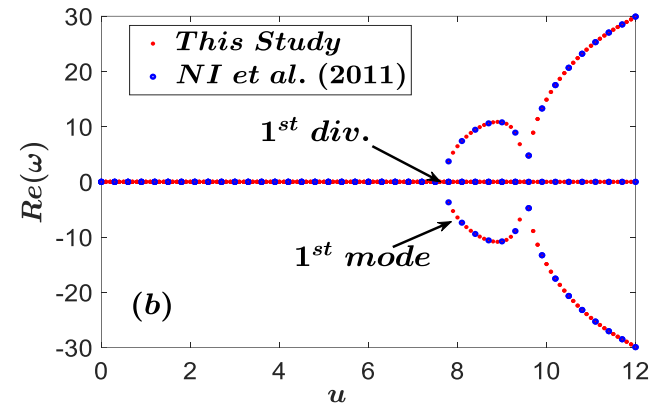
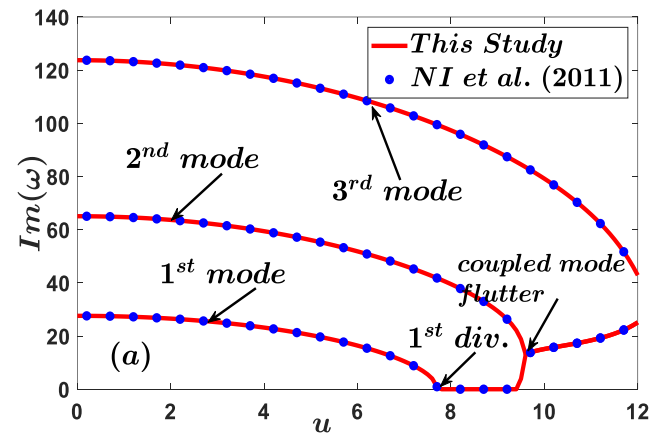
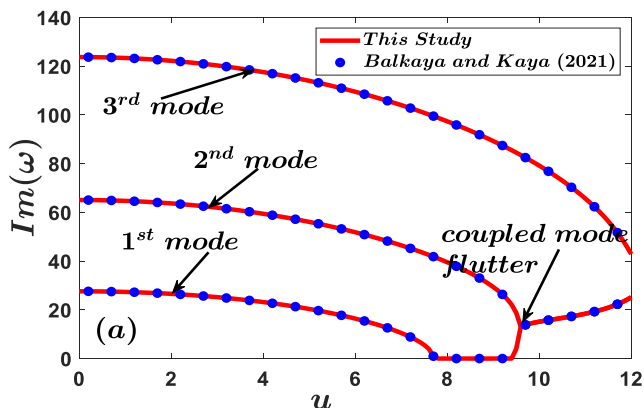


Figure 4. Real and imaginary parts of the three-mode frequencies for a classical pipe carrying fluid resting on two elastic foundations ($k_w = 200, k_g = 3$)



3.2 Effect of fluid flow velocity

The impact of flow velocity on the first four-mode vibration of the uniform porosity AFGM pipe, which conveys fluid, is presented in this subsection, as shown in Table 2 and Figure 4. In the calculation, the parameters used were: $\beta = 0.4$, $\lambda = 0.2$, $\rho = 1$, $\alpha_E = 1.5$, $k_w = 10$, and $k_g = 10$.

This Table shows that dimensionless velocity inversely affects the first three natural frequencies (i.e., the frequencies lower as velocity grows and vice versa). As flow velocity increased, the pipe stiffness decreased, resulting in a drop in natural frequencies.

Table 2. Influence of variable flow velocity on dimensionless vibration frequency

Mode No.	Dimensionless Velocity u				
	0	0.5	1	2	3
ω_1	27.5885	27.5201	27.3137	26.4788	25.0504
ω_2	72.2503	72.1747	71.9478	71.0373	69.5091
ω_3	138.556	138.476	138.236	137.271	135.657
ω_4	226.667	226.585	226.337	225.345	223.687

Figure 5 presents the complex parts of the first three modes of a uniform porosity AFG pipe as a function of fluid velocity. Several phenomena emerge with increasing fluid velocity, including the divergence of the first mode—where the $Im(\omega)$ of the first mode becomes zero—at a specific velocity known as the buckling critical speed, as well as coupling between the 1st and 2nd modes and between the 2nd and 3rd modes at distinct velocities. The divergence of the 1st mode occurs at $u=7.04$, while the coupling between the first and second frequency is observed at $u=9.77$. Whenever the $Im(\omega)$ of the 1st and 2nd frequencies merge, their real parts diverge into two branches, resulting in flutter instability at $u=9.77$. Moreover, when $u=12.54$, the 2nd and 3rd modes are coupled, indicating the second flutter speed.

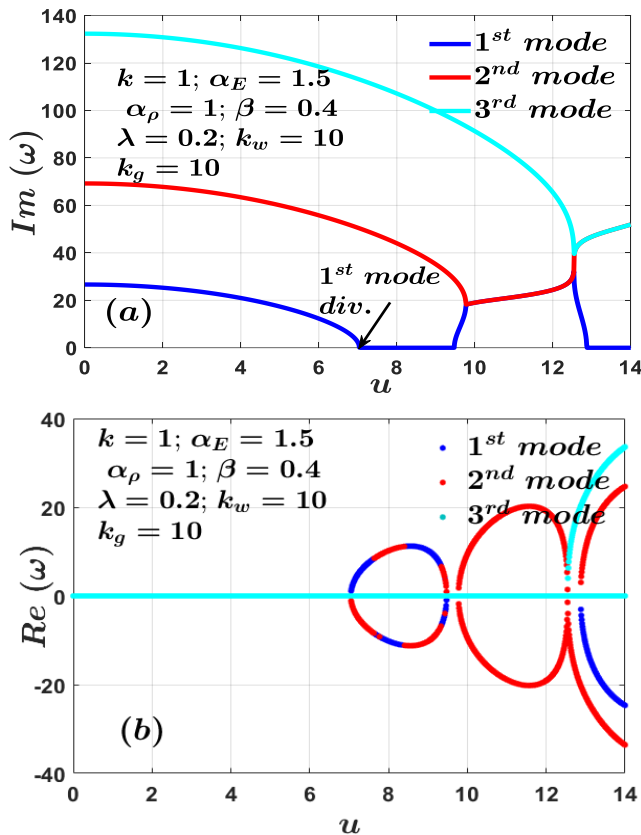


Figure 5. First three-mode vibration frequency versus flow velocity, (a) imaginary, (b) real part frequencies

3.3 Power-index (k) influence

This subsection illustrates the impact of the material gradient on the vibration frequencies of porosity AFGM pipe. The dimensionless frequencies for various gradient indices (k) are shown in Table 3. The Table indicates that the non-dimensional frequency drops as the material index k rises. This reduction occurs because the proportion of ceramic material

within the pipe decreases with the gradient index, leading to a corresponding decrease in frequency.

Table 3. First four dimensionless vibration frequencies at different power indices

Freq. No.	Power Index				
	0	0.5	1	2	5
ω_1	29.4659	28.3821	27.3137	25.6274	24.2504
ω_2	78.3052	74.7394	71.9478	68.5571	65.2025
ω_3	151.1182	143.5160	138.236	132.4846	126.698

Additionally, Figure 6 depicts the variation curves of the non-dimensional frequency for the first mode, with three different values of k (*i. e.* $k = 0.5, 1, \text{ and } 2$), as a function of axial flow speed. The figure illustrates how the eigenvalues of real and imaginary parts are affected by flow velocity. The analysis shows that when the fluid velocity u is less than the critical buckling velocity (first divergence), the imaginary part of the first-order mode eigenvalues of the pipe gradually decreases with increasing axial fluid speed, while the real frequency remains zero. Furthermore, it is evident that as the power-law gradient rises, the critical velocity diminishes. Moreover, the vibration frequency decreases as the gradient exponent k increases. This is attributed to the greater proportion of metal, which has a lower modulus of elasticity than the ceramic material, resulting in reduced pipe stiffness.

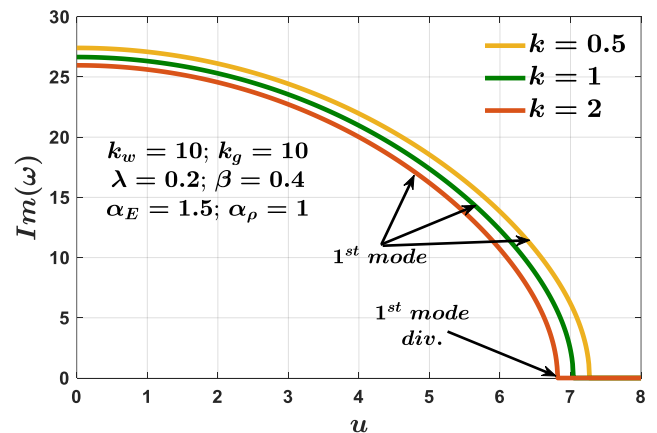


Figure 6. Variation in first-order frequency of an AFGM pipe with different gradient indices

3.4 Effect of modulus of elasticity ratio α_E

Table 4. Natural frequencies for different power- index k and elastic modulus ratio

α_E	Fr. No.	Gradient Index (k)				
		0	0.5	1	2	5
0.25	1	15.498	18.494	20.909	23.935	25.832
	2	37.036	46.756	52.727	59.362	65.410
	3	67.530	87.621	98.536	110.22	122.09
0.5	1	19.147	20.815	22.268	24.197	25.502
	2	48.226	53.593	57.181	61.263	65.165
	3	90.649	101.81	108.39	115.45	122.76
1	1	24.853	24.853	24.853	24.853	24.853
	2	65.033	65.033	65.033	65.033	65.033
	3	124.60	124.60	124.60	124.60	124.60
2	1	33.446	31.549	29.653	26.468	23.704
	2	89.6314	83.3374	78.2284	71.8343	65.545
	3	173.62	160.11	150.31	139.47	128.81

This subsection discusses the impact of the modulus ratio (α_E) on the natural non-dimensional frequencies. Table 4 illustrates the influence of the ratio of modules (E_L/E_R) for $\beta = 0.4$, $\lambda = 0.2$, $\alpha_\rho = 1$, $k_w = 10$, and $k_g = 10$. It is clear that from Table 4 when $\alpha_E < 1$, the natural frequency increased with the growth of the gradient index, and when $\alpha_E = 1$ the natural frequency is constant because the pipe has a homogenous material in any position of the pipe, but this trend is vice versa when $\alpha_E > 1$.

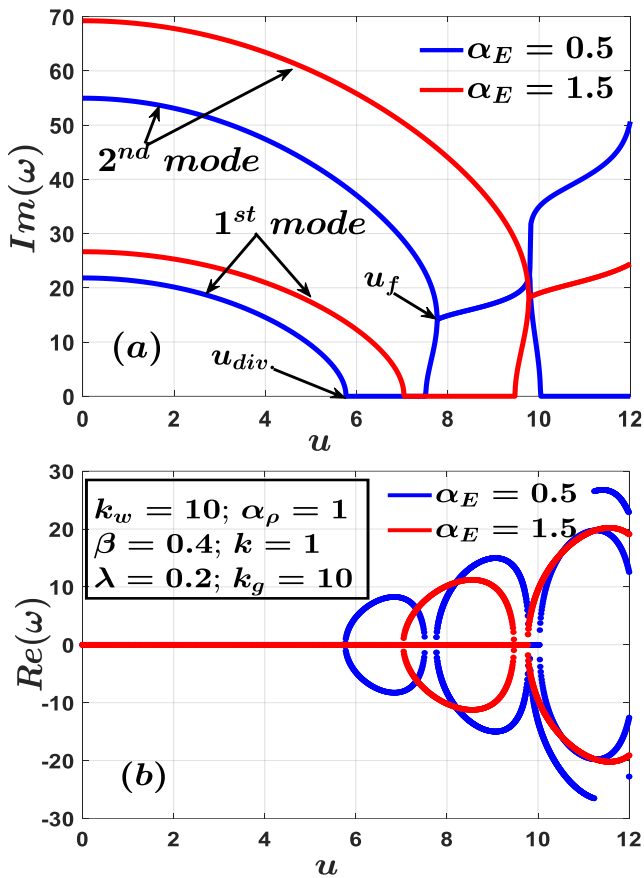


Figure 7. Effect of modulus ratio on first and second-order frequencies at various flow velocities

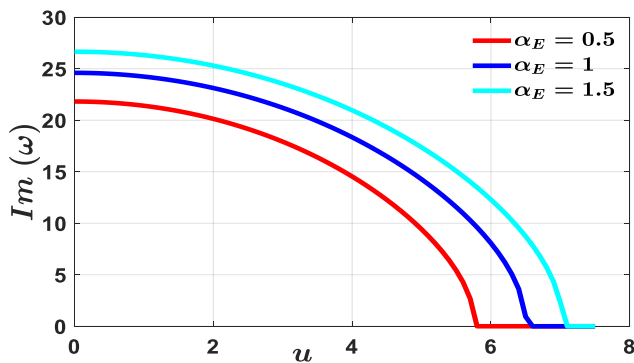


Figure 8. First frequency variation against various modulus ratios

In Figure 7, the fundamental two-order frequency variations are plotted against changes in the flow velocity with two variables of α_E ($\alpha_E = 0.5$ and $\alpha_E = 1.5$). Also, in Figure 8, the effect of three different values of α_E on first frequency is presented. As can be seen, the system's fundamental frequency decreases uniformly with an increase in axial velocity. Up to

the point of axial divergence velocity (u_d), the fundamental frequency drops to zero, after which the system undergoes divergence within a specific range of axial velocities. Additionally, it is noted that as the elastic modulus ratio (α_E) increases, the 1st order frequency, and the divergence system velocity also rises. This phenomenon can be attributed to the primary effect of the elastic modulus on the pipe's stiffness matrix. Thus, raising the elastic parameter enhances the pipe stiffness. Consequently, as the elastic modulus ratio (α_E) increases, the system's resistance to divergence improves, resulting in higher divergence speeds. An increased elastic modulus parameter results in a structurally stiffer system.

3.5 Impact of foundation parameter

In this subsection, the fundamental frequencies of double-simple functional grade (FG) pipes carrying fluids are investigated with various foundation parameters (k_w, k_g). In Figures 9(a) and 9(b), the first frequency for the different elastic layer (k_w) and shear layer (k_g) parameters are presented. These figures show that a rise in coefficient foundation leads to an increase in fundamental frequencies. It can also be seen that, compared to elastic (k_w) bed, the shear (k_g) bed has a more pronounced effect on the system's stability.

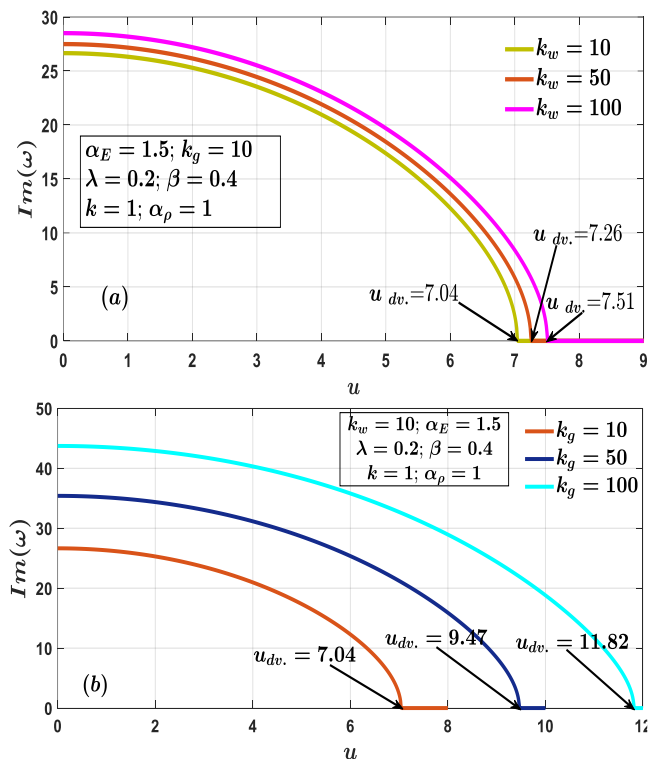


Figure 9. Influence of fluid velocity on the fundamental frequency relative to the elastic foundation parameters, (a) Winkler parameter k_w , (b) Shear parameter k_g

In Figure 10, the effects of foundation coefficients on the static instability boundaries in the $\omega - u$ plane are illustrated. Incorporating the foundation into the system improves its effective stiffness, leading to increased stability compared to a system without foundation. This is due to the stiffness matrix coefficients; as the foundation parameters increase, the system stiffness improves, resulting in enhanced stability. It can be

seen that when increasing (k_w and k_g), the FG pipe stiffness and the critical flow velocity increase. Furthermore, this figure shows that the dimensionless frequency reduces as fluid velocity grows.

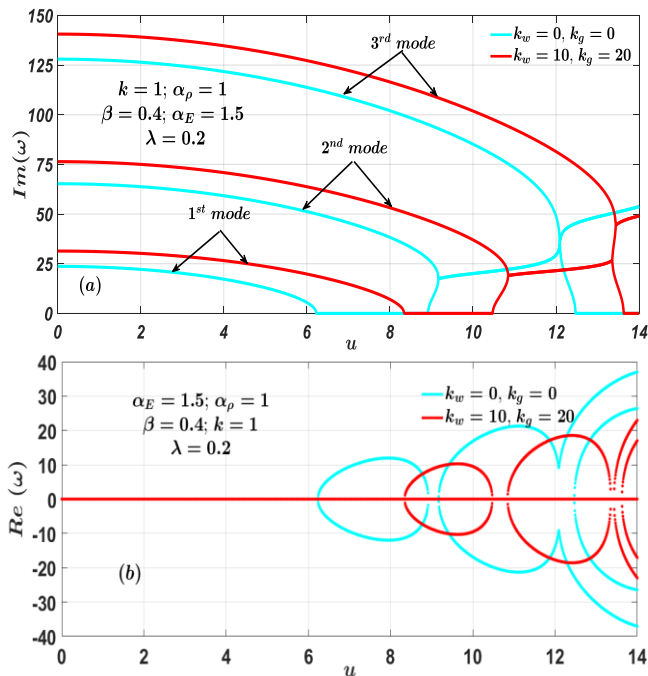


Figure 10. The first three modes of C-C fluid conveying AFG pipe with and without elastic foundation

4. CONCLUSIONS

This paper explores the stability of uniform porosity (AFG) pipe translating fluid. The material properties of the pipe exhibit a power-law distribution along the axial direction, and the pipe was modelled using the Euler-Bernoulli theory (EBT). Numerical simulations are conducted using the GM, and the results are confirmed by comparison with existing literature. Additionally, the study thoroughly examines the coupling effects of the FG material characteristics and various parameters on the dynamic behaviour of the pipe. This analysis led to the following conclusions:

1. When the modulus ratio (α_E) is less than 1, an increase in the power index (k) results in a rise in frequency. Conversely, when (α_E) is greater than 1, an increase in (k) leads to a decrease in frequency. No change in frequency is observed when (α_E) equals 1.
2. When accounting for both parameters of the Pasternak Foundation (k_w, k_g), an increase in natural frequency and critical velocity is observed.
3. The AFG pipe remains stable at low flow velocities, but its stability deteriorates as the internal fluid velocity increases. When the flow velocity surpasses a critical threshold, the pipe experiences divergence instability.
4. In AFG pipes, the fundamental frequency and divergence velocity for structural stability increment as the elastic modulus ratio (α_E) increases.

This analysis provides valuable insights for engineers and researchers in optimizing the design of fluid-conveying pipes to minimize undesirable vibrations and prevent instability in critical applications.

As suggestions for the future direction, the current study can

be enhanced with a temperature gradient effect, nonlinear effects, complex support, and an external excitation force.

REFERENCES

- [1] Heshmati, M., Daneshmand, F., Amini, Y. (2023). Vibration and stability analysis of functionally graded elliptical pipes conveying fluid with flow velocity profile modification. *Engineering with Computers*, 39: 1537-1552. <https://doi.org/10.1007/s00366-021-01541-1>
- [2] Giacobbi, D.B., Semler, C., Païdoussis, M.P. (2020). Dynamics of pipes conveying fluid of axially varying density. *Journal of Sound and Vibration*, 473: 115202. <https://doi.org/10.1016/j.jsv.2020.115202>
- [3] Dagli, B.Y., Ergut, A. (2019). Dynamics of fluid conveying pipes using Rayleigh theory under non-classical boundary conditions. *European Journal of Mechanics-B/Fluids*, 77: 125-134. <https://doi.org/10.1016/j.euromechflu.2019.05.001>
- [4] Xu, Y., Zhang, L., Wei, H., Zhang, Z., Yang, F., Hu, H., Hu, Y. (2023). Nonlinear dynamics of viscoelastic fluid-conveying pipe installed within uniform external cross flow by pipe clamps. *Applied Ocean Research*, 135: 103547. <https://doi.org/10.1016/j.apor.2023.103547>
- [5] Zhao, Q., Liu, W., Yu, W., Cai, F. (2024). Dynamics of a fluid-conveying pipe by a hybrid method combining differential transformation and Galerkin discretization. *Iranian Journal of Science and Technology, Transactions of Mechanical Engineering*, 48(2): 647-659. <https://doi.org/10.1007/s40997-023-00680-8>
- [6] Ma, Y., You, Y., Chen, K., Feng, A. (2024). Analysis of vibration stability of fluid conveying pipe on the two-parameter foundation with elastic support boundary conditions. *Journal of Ocean Engineering and Science*, 9(6): 616-629. <https://doi.org/10.1016/j.joes.2022.11.002>
- [7] Li, M., Zhao, X., Li, X., Chang, X.P., Li, Y.H. (2018). Stability analysis of oil-conveying pipes on two-parameter foundations with generalized boundary condition by means of Green's functions. *Engineering Structures*, 173: 300-312. <https://doi.org/10.1016/j.engstruct.2018.07.001>
- [8] Askarian, A.R., Permoon, M.R., Shakouri, M. (2020). Vibration analysis of pipes conveying fluid resting on a fractional Kelvin-Voigt viscoelastic foundation with general boundary conditions. *International Journal of Mechanical Sciences*, 179: 105702. <https://doi.org/10.1016/j.ijmecsci.2020.105702>
- [9] Balkaya, M., Kaya, M.O. (2021). Analysis of the instability of pipes conveying fluid resting on two-parameter elastic soil under different boundary conditions. *Ocean Engineering*, 241: 110003. <https://doi.org/10.1016/j.oceaneng.2021.110003>
- [10] Wu, N., Zhao, Y., Guo, Q., Liu, Y. (2020). The effect of two-parameter of Pasternak foundations on the dynamics and stability of multi-span pipe conveying fluids. *Advances in Mechanical Engineering*, 12(11): 1687814020974530. <https://doi.org/10.1177/1687814020974530>
- [11] Saleh, B., Jiang, J., Fathi, R., Al-Hababi, T., Xu, Q., Wang, L., Ma, A. (2020). 30 Years of functionally graded materials: An overview of manufacturing methods. Applications and Future Challenges. *Composites Part B:*

- Engineering, 201: 108376. <https://doi.org/10.1016/j.compositesb.2020.108376>
- [12] Awrejcewicz, J., Kurpa, L., Shmatko, T. (2018). Linear and nonlinear free vibration analysis of laminated functionally graded shallow shells with complex plan form and different boundary conditions. *International Journal of Non-Linear Mechanics*, 107: 161-169. <https://doi.org/10.1016/j.ijnonlinmec.2018.08.013>
- [13] Elaikh, T.E., Abd, N.M., Ali, A.H. (2023). Dynamic characteristics of cracked simply supported bidirectional functionally graded Rayleigh beam. *Results in Materials*, 19: 100441. <https://doi.org/10.1016/j.rinma.2023.100441>
- [14] Jha, D.K., Kant, T., Singh, R.K. (2013). A critical review of recent research on functionally graded plates. *Composite Structures*, 96: 833-849. <https://doi.org/10.1016/j.compstruct.2012.09.001>
- [15] Cao, J. (2022). Instability analysis of fluid-conveying functionally graded thin-walled pipes on random elastic foundations. *Journal of Physics: Conference Series*, 2230(1): 012036. <https://doi.org/10.1088/1742-6596/2230/1/012036>
- [16] Ma, T., Mu, A. (2022). Analysis of nonlinear vibration of functionally graded simply supported fluid-conveying microtubes subjected to transverse excitation loads. *Micromachines*, 13(12): 2114. <https://doi.org/10.3390/mi13122114>
- [17] Guo, Q., Liu, Y., Chen, B., Zhao, Y. (2021). An efficient stochastic natural frequency analysis method for axially varying functionally graded material pipe conveying fluid. *European Journal of Mechanics-A/Solids*, 86: 104155. <https://doi.org/10.1016/j.euromechsol.2020.104155>
- [18] Ihmood, S.M., Al-Umar, M. (2022). Free vibration of new type functionally graded materials pipe conveying fluid using differential quadrature method. *AIP Conference Proceedings*, 2386(1): 080012. <https://doi.org/10.1063/5.0066803>
- [19] El, T.E., Ihmood, S.M. (2019). Differential quadrature method for dynamic behavior of function graded materials pipe conveying fluid on visco-elastic foundation. *University of Thi-Qar Journal for Engineering Sciences*, 10(1): 50-64. [https://doi.org/10.31663/tqujes.10.1.352\(2019\)](https://doi.org/10.31663/tqujes.10.1.352(2019))
- [20] Selmi, A., Hassis, H. (2021). Vibration analysis of post-buckled fluid-conveying functionally graded pipe. *Composites Part C: Open Access*, 4: 100117. <https://doi.org/10.1016/j.jcomc.2021.100117>
- [21] Deng, J., Liu, Y., Zhang, Z., Liu, W. (2017). Stability analysis of multi-span viscoelastic functionally graded material pipes conveying fluid using a hybrid method. *European Journal of Mechanics-A/Solids*, 65: 257-270. <https://doi.org/10.1016/j.euromechsol.2017.04.003>
- [22] Wang, Z.M., Liu, Y.Z. (2016). Transverse vibration of pipe conveying fluid made of functionally graded materials using a symplectic method. *Nuclear Engineering and Design*, 298: 149-159. <https://doi.org/10.1016/j.nucengdes.2015.12.007>
- [23] An, C., Su, J. (2017). Dynamic behavior of axially functionally graded pipes conveying fluid. *Mathematical Problems in Engineering*, 2017(1): 6789634. <https://doi.org/10.1155/2017/6789634>
- [24] Zhao, Y., Hu, D., Wu, S., Long, X., Liu, Y. (2021). Dynamics of axially functionally graded conical pipes conveying fluid. *Journal of Mechanics*, 37: 318-326. <https://doi.org/10.1093/jom/ufaa030>
- [25] Elaikh, T.E., Abed, N.M., Ebrahimi-Mamaghani, A. (2020). Free vibration and flutter stability of interconnected double graded micro pipes system conveying fluid. *IOP Conference Series: Materials Science and Engineering*, 928(2): 022128. <https://doi.org/10.1088/1757-899X/928/2/022128>
- [26] Zhu, B., Chen, X.C., Guo, Y., Li, Y.H. (2021). Static and dynamic characteristics of the post-buckling of fluid-conveying porous functionally graded pipes with geometric imperfections. *International Journal of Mechanical Sciences*, 189: 105947. <https://doi.org/10.1016/j.ijmecsci.2020.105947>
- [27] Li, N., Zhang, H., Bai, C. (2023). Effects of pores on nonlinear vibration and post buckling behavior of functionally graded material pipes conveying fluid. *Proceedings of the Institution of Mechanical Engineers, Part C: Journal of Mechanical Engineering Science*, 237(18): 4187-4202. <https://doi.org/10.1177/0954406220982015>
- [28] Zhou, J., Chang, X., Li, Y. (2022). Nonlinear vibration analysis of functionally graded flow pipelines under generalized boundary conditions based on homotopy analysis. *Acta Mechanica*, 233(12): 5447-5463. <https://doi.org/10.1007/s00707-022-03391-4>
- [29] Khodabakhsh, R., Saidi, A.R., Bahaadini, R. (2022). Exact closed-form solution for nonlinear stability analysis of porous functionally graded pipes conveying fluid under various boundary conditions. *Journal of Vibration Engineering & Technologies*, 10(8): 2877-2891. <https://doi.org/10.1007/s42417-022-00524-w>
- [30] Mao, X.Y., Jing, J., Ding, H., Chen, L.Q. (2023). Dynamics of axially functionally graded pipes conveying fluid. *Nonlinear Dynamics*, 111(12): 11023-11044. <https://doi.org/10.1007/s11071-023-08470-2>
- [31] Elaikh, T.E., Agboola, O.O.O. (2022). Investigation of transverse vibration characteristics of cracked axially moving functionally graded beam under thermal load. *Trends in Sciences*, 19(23): 1349. <https://doi.org/10.48048/tis.2022.1349>
- [32] Majeed, S.H., Elaikh, T.E., Uгла, A.A.H. (2024). Reformulated strain gradient (RSG) elasticity theory for free vibration of thermal bi-directional FG microbeam. *Jurnal Teknologi (Sciences & Engineering)*, 86(2): 123-134. <https://doi.org/10.11113/jurnalteknologi.v86.21047>
- [33] Rao, S.S. (2006). *Vibration of Continuous Systems*. John Wiley & Sons, Inc. <https://doi.org/10.1002/9780470117866>
- [34] Ebrahimi-Mamaghani, A., Sotudeh-Gharebagh, R., Zarghami, R., Mostoufi, N. (2022). Thermo-mechanical stability of axially graded Rayleigh pipes. *Mechanics Based Design of Structures and Machines*, 50(2): 412-441. <https://doi.org/10.1080/15397734.2020.1717967>
- [35] Elaikh, T.E., Abed, N.M. (2019). Stability of FG material micro-pipe conveying fluid. *International Journal of Energy and Environment*, 10(4): 211-221.
- [36] Ni, Q., Zhang, Z.L., Wang, L. (2011). Application of the differential transformation method to vibration analysis of pipes conveying fluid. *Applied Mathematics and Computation*, 217(16): 7028-7038. <https://doi.org/10.1016/j.amc.2011.01.116>

NOMENCLATURE

A	cross-sectional area m ²
AFG	axially functionally graded
C-C	clamped-clamped
DTM	differential transformation method
<i>E</i>	modulus of elasticity GPa
FEM	finite element method
G	modulus of rigidity GPa
HDQ	harmonic differential quadrature
I	the second moment of inertia m ⁴
k	volume fraction index
<i>k_g</i>	dimensionless shear parameter
<i>k_w</i>	dimensionless elastic parameter
L	pipe length m
<i>m_f</i>	fluid mass per unit length kg. L ⁻¹
<i>r_i</i>	inner radius mm
<i>r_o</i>	outer radius mm

<i>T</i>	kinetic energy
t	time s.
U	fluid velocity m.s ⁻¹
<i>U_S</i>	strain energy
<i>W</i>	virtual work

Greek symbols

β	mass density ratio
η	transverse displacement dimensionless
λ	porosity factor
ξ	axial displacement dimensionless
ω	non-dimensional natural frequency

Subscripts

o	left side
R	right side